Published in "The Journal of Physical Chemistry Letters 5(1): 80–84, 2014"
which should be cited to refer to this work.

Supporting Information

Real Time Determination of the Electronic Structure of Unstable Reaction Intermediate During Au_2O_3 Reduction

Jakub Szlachetko[1,2,], Jacinto Sá[1,3], Maarten Nachtegaal[1], Urs Hartfelder[1,4], Jean-Claude Dousse[5], Joanna Hoszowska[5], Daniel Luis Abreu Fernandes[6], Hongqing Shi[7], Catherine Stampfl[7]

Experimental setup

The in-situ time-resolved RIXS experiments were performed at the SuperXAS beamline of the Swiss Light Source, Paul Scherrer Institute, Switzerland. The X-rays delivered from a super cooled bending magnet were collimated with a Rh mirror and monochromatized with a pair of Si(111) crystals. Downstream from the monochromator, the X-ray beam was focused by means of a toroidal Rh mirror. The beam size on the sample was 100 x 100 μm^2 with photon flux of about 10^{12} ph/sec. The incident X-ray energy was tuned around the Au L_3 edge (11919eV) and the $L_{\alpha 1}$ X-ray fluorescence from the sample was recorded by means of a von Hamos type spectrometer[1]. The spectrometer was equipped with cylindrically bent Ge(660) crystal and operated at a Bragg angle of around 73°. The diffracted X-rays were recorded by means of strip-type detector with spatial resolution of $50\mu^2$. The overall experimental resolution was 1.9eV,which is significantly lower than the natural broadening of the Au L_3 state that is 5.54eV[3].

For the sample, an Au(III) oxide powder from Alfa Aesar was loaded into a quartz capillary with diameter of 3 mm and 50 μm thick wall. The capillary was connected to a 5%H_2/He gas inlet. During the experiment, the Au(III) powder was heated-up at a ramp of 5 °C per minute. The RIXS planes were collected simultaneously by continuous scanning of the incident X-ray energy and recording intensity of the emitted X-ray fluorescence from the sample.

Chemometric data analysis details

The time-resolved RIXS data were analyzed to determine relative concentration changes of Au(III) oxide and Au(0) during the temperature programmed reduction experiment. The time-resolved RIXS planes were fitted using the Au(III) and Au(0) RIXS data of Fig. 2 in the manuscript as references. The outcome of the fitting for the three different temperatures is presented in Fig. S1. As shown, at initial and final temperatures the fit residuals are of the order of +/- 1%, while for intermediate temperatures a discrepancy in the fitted intensity in the range of -3% to +5% is observed. Moreover, the fit discrepancy is localized around 5d resonance (excitation energy of 11920eV and emission energy of 9713eV) and shows systematic behavior along constant energy transfer. The result implies that at intermediate temperatures the RIXS plane cannot be fitted using only two references and suggests existence of a third component in it. This result was also confirmed by independent component analysis (ICA)[4], which detected the existence of a third statistically independent component.

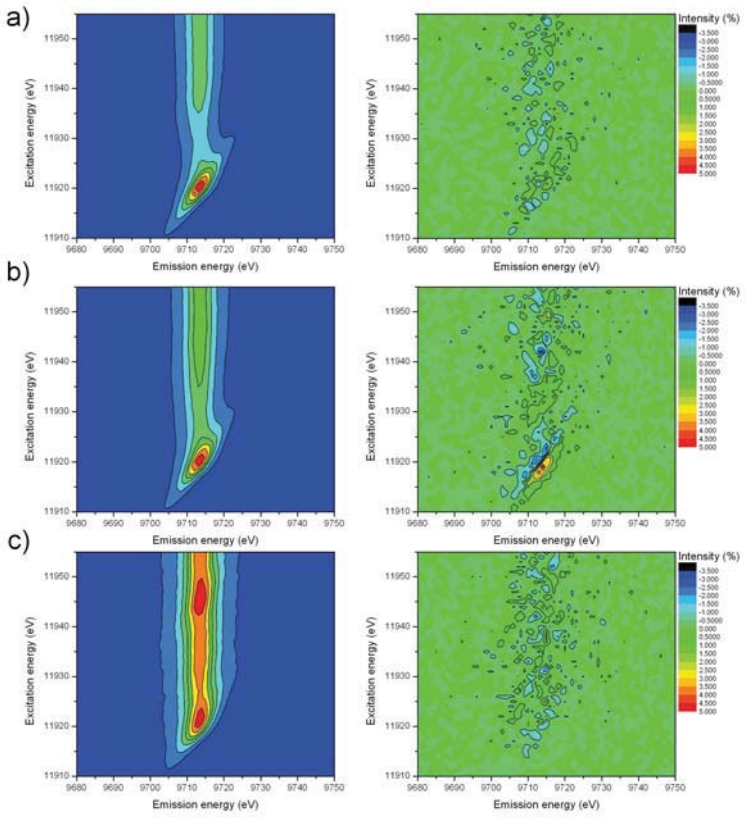

Figure S1. left) Experimental in-situ RIXS spectra of Au at different temperatures, right) residuals of two component least square fitting procedure. Temperatures: a) 20-50 °C, b) 150-200 °C, c) 270-300 °C.

We used a genetic algorithm procedure[5, 6] to find the RIXS spectrum of the intermediate component. The genetic algorithm was implemented using the genetic algorithm graphical user interface of MATLAB. The fitness function uses the following method to determine the fitness value: First, a linear combination of the initial spectrum, the final spectrum and the vector from the population is found so that it minimizes the squared residuals when subtracted from RIXS spectra taken at different times where the intermediate is present. The squared residuals are then returned as the fitness function. Multiple spectra are used to minimize the effect of random noise in a single spectrum on the result. The linear combination was constrained to coefficients between zero and one. Since the spectrum of the intermediate was assumed to contain features also present in

those of the initial and the final state, an initial population was generated with a shape similar to what was expected for the spectrum, i.e., a tangent function in the excitation energy direction and a lorentzian in the emission energy axis. The schematic flow of data analysis employing genetic algorithm procedure is presented in Fig. S2.

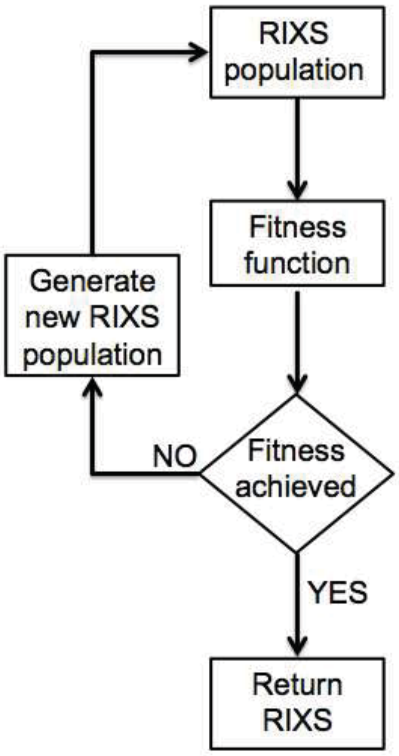

Figure S2. Chart flow for genetic algorithm procedure for extraction of RIXS plane of intermediate Au compound.

Surface calculations for Au_2O on Au_2O_3

The crystal structures of $Au_2O_3$is shown in Fig. S3a), where the calculated lattice constants are 13.06 Å, 10.68 Å and 4.04 Å, for the a, b, and c vectors, respectively. These values are in good agreement, but slightly larger than the experimental values which are 12.83 Å, 10.52 Å and 3.84 Å, respectively. That of Au_2O is shown in Fig. S3b), where

the calculated lattice constant is 4.80 Å, in good agreement with other *ab initio* values. These values are reported in our earlier publication[7].

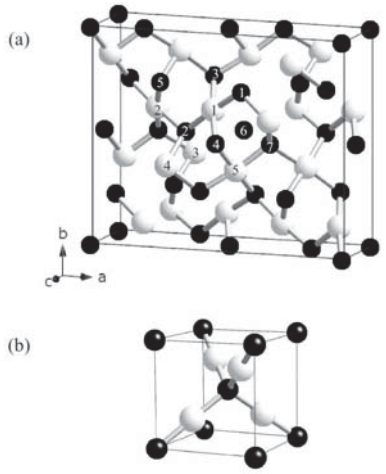

Figure S3. Atomic structure of (a) the Au_2O_3 unit cell and (b) the cuprite bulk Au_2O unit cell. Oxygen and gold atoms are indicated by the small and large spheres, respectively.

From the present experimental results, the detected short-lived Au_2O compound has a lattice constant considerably larger than the theoretical value (of 4.80 Å), namely 5.3 Å. The present experiment also shows that the reduction of Au_2O_3 is a shell-to-core process where Au_2O exists as a thin layer terminating the Au_2O_3 core structure. We therefore investigate theoretically, through density functional theory (DFT) calculations[8] using the generalized gradient approximation[9], whether a thin layer of $Au_2O(001)$, under this tensile strain, can be stabilized on the Au_2O_3 (001) surface.

In particular, on considering the lattice constants involved (i.e. substrate Au_2O_3) and experimentally measured strained Au_2O layer, it is observed that a very close epitaxial match exists for $(5x2)Au_2O(001)$ on a $(2x1)Au_2O_3(001)$ surface. Comparing the experimental lattice constants corresponding to this, it represents a mismatch of only -3.3% and -0.8% (compressive strain) in the a and b lattice directions, respectively (i.e. 5x5.3Å = 26.5 Å vs 2x12.83 Å = 25.66 Å and 2x5.3 Å = 10.6 Å vs 10.52 Å). This

corresponds to a situation where there are ten surface unit cells of $Au_2O(001)$ on two surface unit cells of $Au_2O_3(001)$.

To investigate the relative stability of a thin layer of $Au_2O(001)$ on $Au_2O_3(001)$ (see Figs. S4a and S4b) as compared to the unreconstructed $Au_2O_3(001)$ surface (Fig. S4c), we use the approach of *ab initio* atomistic thermodynamics[10]. This approach predicts the stability of surface structures for various pressure and temperature conditions.

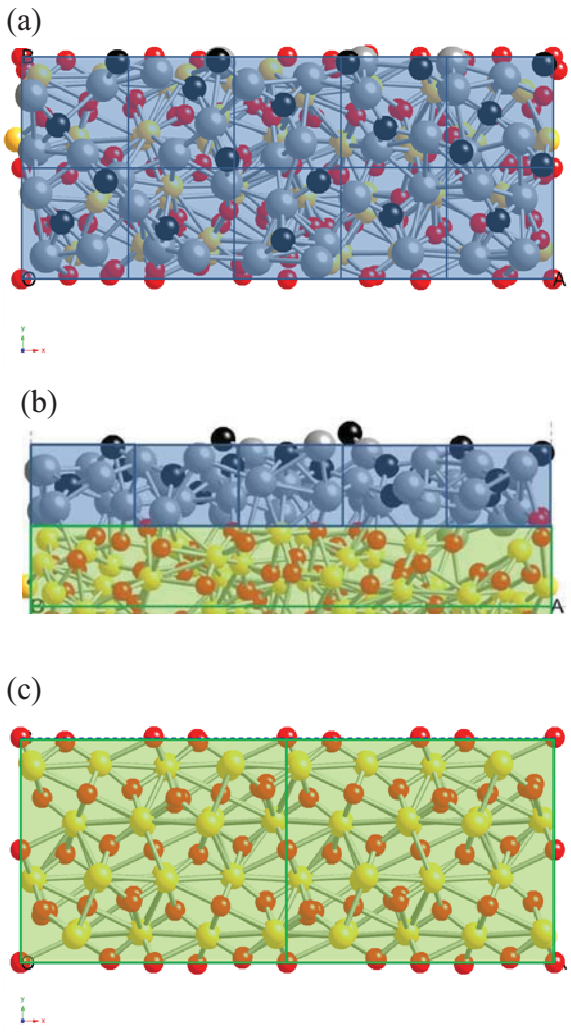

Figure S4. (a) Top view of the atomic structure of Au_2O on Au_2O_3 and (b) the side view. The layer of Au_2O is shaded grey. Oxygen and gold atoms are indicated by the small and larger spheres, respectively. (c) The top view of the two surface unit cells of Au_2O_3 (001).

Calculation details

The wave functions are expanded in a plane-wave basis set with an energy cutoff of 29.40 Ry (500 eV). The repeating slabs are separated by 15 Å of vacuum space. We allow full atomic relaxation of all gold and oxygen atoms. The final forces on the atoms are less than 0.01 eV/Å. For the **k**-point sampling, a 1x2x1 mesh of (Γ-centered) points is used for the (2x1) Au_2O_3 surface unit cell (SUC), which generates 2 **k** points in the irreducible surface Brillouin zone (BZ) for the BZ integration. Identical **k** points are used for all of the surface structures studied to maximize the accuracy. A Gaussian function is used with a temperature broadening of k_BT^{el}=0.2 eV to improve the convergence, and the total energy is extrapolated to zero temperature. The PAW potential is generated taking scalar relativistic corrections into account.

The free energy of formation for the Au_2O_3-Au_2O system depends on the stoichiometry, and the environmental atmosphere, through the atomic chemical potentials and is given by,

$$F(T,p) = 1/A(G-N_{Au}\,\mu_{Au} - N_O\,\mu_O) = 1/A[G-N_{Au}\,(\,½\,E_{Au2O3} - {}^3/_2E\,\mu_O) - N_O\mu_O]$$

with the constraint $2\mu_{Au} + 3\mu_O = \mu_{Au2O3}$. G is the Gibbs free energy of the Au_2O_3-Au_2O system, where the total energy is the predominant term in G. We refer to Reuter and Scheffler work[10] for more details on this approach. A is the corresponding area of the surface unit cell. N_{Au} and N_O are the numbers of the gold and oxygen atoms in the system, respectively. μ_{Au} and μ_O are the chemical potentials of each species, respectively. μ_{Au2O3} is the chemical potential per Au_2O_3 unit, which is approximately represented by the total energy of bulk Au_2O_3, E_{Au2O3}.

Results and discussion

Figure S5 shows the formation energy as a function of the oxygen chemical potential, which is correlated to oxygen gas pressure and the temperature. The zero of formation energy is taken as that of the Au_2O_3 (001) surface (i.e. two layers of Au_2O_3). The vertical full line (energy zero of $\lambda\mu_O$) represents "O-rich" conditions where μ_O is equal to that of an O atom in the O_2 molecule. The dashed vertical line indicates the heat-of-formation of Au_2O_3 (per O atom), which is calculated to be -0.173 eV/Oatom (or -0.519 eV per stoichiometric unit)[7]. For values of $\lambda\mu_O$ lower than that, Au_2O_3 becomes unstable.

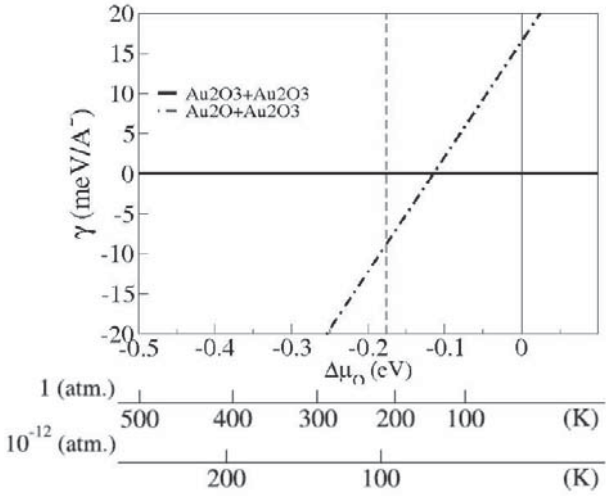

Figure S5. Formation energy of Au_2O on Au_2O_3 (dot-dashed line), compared to that of unreconstructed Au_2O_3 (001) (taken as the energy zero). The vertical full line (energy zero of $\lambda\mu_O$) represents "O-rich" conditions where the μ_O is equal to that of an O atom in O_2. The dashed vertical line indicates the

It can be seen from Fig. S5 that for values of $\lambda\mu_O$ greater than (less negative) about -0.11 eV (low tempertures) that the unreconstructed Au_2O_3 structure is more stable than the surface structure with a thin layer of Au_2O. But for values less (more negative) than -0.11 eV (corresponding to increasing temperature), it becomes favorable to form a thin layer

of Au_2O on the surface. This is indicated by the sloping dot-dashed line having a more negative (favorable) formation energy in this range of O-chemical potential than the Au_2O_3 surface.

This result is consistent with the experimental results that detect the presence of strained Au_2O on the surface of Au_2O_3, and predicts that in some parts of the sample, such structures can be stabilized.

Au_2O Feff input file:

```
CONTROL 1 1 1 1 1 1
PRINT 1 0 0 0 0 0
EDGE L3
S02 1.0
SCF 4 0 30 0.2 1
EXCHANGE 0 1.5 -1.5 0
COREHOLE None
LDOS -30 20 0.5
XANES 3.5 0.03 0.5
FMS 5.04894 0
POTENTIALS
0 79 Au 3 3 0.0010
1 79 Au 3 3 4.0
2 8 O 1 1 2.0
ATOMS
 0.00000   0.00000   0.00000   0 Au1          0.00000   0
-1.32500  -1.32500   1.32500   2 O1           2.29497   1
 1.32500   1.32500  -1.32500   2 O1           2.29497   2
 2.65000   2.65000   0.00000   1 Au1          3.74767   3
-2.65000   2.65000   0.00000   1 Au1          3.74767   4
 2.65000  -2.65000   0.00000   1 Au1          3.74767   5
-2.65000  -2.65000   0.00000   1 Au1          3.74767   6
 2.65000   0.00000   2.65000   1 Au1          3.74767   7
-2.65000   0.00000   2.65000   1 Au1          3.74767   8
 0.00000   2.65000   2.65000   1 Au1          3.74767   9
 0.00000  -2.65000   2.65000   1 Au1          3.74767  10
 2.65000   0.00000  -2.65000   1 Au1          3.74767  11
-2.65000   0.00000  -2.65000   1 Au1          3.74767  12
 0.00000   2.65000  -2.65000   1 Au1          3.74767  13
 0.00000  -2.65000  -2.65000   1 Au1          3.74767  14
```

-1.32500	3.97500	1.32500	2 O1	4.39453	15
3.97500	-1.32500	1.32500	2 O1	4.39453	16
-3.97500	1.32500	-1.32500	2 O1	4.39453	17
1.32500	-3.97500	-1.32500	2 O1	4.39453	18
1.32500	1.32500	3.97500	2 O1	4.39453	19
-1.32500	-1.32500	-3.97500	2 O1	4.39453	20
5.30000	0.00000	0.00000	1 Au1	5.30000	21
-5.30000	0.00000	0.00000	1 Au1	5.30000	22
0.00000	5.30000	0.00000	1 Au1	5.30000	23
0.00000	-5.30000	0.00000	1 Au1	5.30000	24
0.00000	0.00000	5.30000	1 Au1	5.30000	25
0.00000	0.00000	-5.30000	1 Au1	5.30000	26
3.97500	3.97500	1.32500	2 O1	5.77554	27
-3.97500	1.32500	3.97500	2 O1	5.77554	28
1.32500	-3.97500	3.97500	2 O1	5.77554	29
-3.97500	-3.97500	-1.32500	2 O1	5.77554	30
-1.32500	3.97500	-3.97500	2 O1	5.77554	31
3.97500	-1.32500	-3.97500	2 O1	5.77554	32
5.30000	2.65000	2.65000	1 Au1	6.49115	33
-5.30000	2.65000	2.65000	1 Au1	6.49115	34
2.65000	5.30000	2.65000	1 Au1	6.49115	35
-2.65000	5.30000	2.65000	1 Au1	6.49115	36
5.30000	-2.65000	2.65000	1 Au1	6.49115	37
-5.30000	-2.65000	2.65000	1 Au1	6.49115	38
2.65000	-5.30000	2.65000	1 Au1	6.49115	39
-2.65000	-5.30000	2.65000	1 Au1	6.49115	40
2.65000	2.65000	5.30000	1 Au1	6.49115	41
-2.65000	2.65000	5.30000	1 Au1	6.49115	42
2.65000	-2.65000	5.30000	1 Au1	6.49115	43
-2.65000	-2.65000	5.30000	1 Au1	6.49115	44
5.30000	2.65000	-2.65000	1 Au1	6.49115	45
-5.30000	2.65000	-2.65000	1 Au1	6.49115	46
2.65000	5.30000	-2.65000	1 Au1	6.49115	47
-2.65000	5.30000	-2.65000	1 Au1	6.49115	48
5.30000	-2.65000	-2.65000	1 Au1	6.49115	49
-5.30000	-2.65000	-2.65000	1 Au1	6.49115	50
2.65000	-5.30000	-2.65000	1 Au1	6.49115	51
-2.65000	-5.30000	-2.65000	1 Au1	6.49115	52
2.65000	2.65000	-5.30000	1 Au1	6.49115	53
-2.65000	2.65000	-5.30000	1 Au1	6.49115	54
2.65000	-2.65000	-5.30000	1 Au1	6.49115	55
-2.65000	-2.65000	-5.30000	1 Au1	6.49115	56
-1.32500	-1.32500	6.62500	2 O1	6.88490	57
1.32500	1.32500	-6.62500	2 O1	6.88490	58
-6.62500	-1.32500	1.32500	2 O1	6.88490	59
-1.32500	-6.62500	1.32500	2 O1	6.88490	60

-3.97500	-3.97500	3.97500	2 O1	6.88490	61
6.62500	1.32500	-1.32500	2 O1	6.88490	62
1.32500	6.62500	-1.32500	2 O1	6.88490	63
3.97500	3.97500	-3.97500	2 O1	6.88490	64
5.30000	5.30000	0.00000	1 Au1	7.49533	65
-5.30000	5.30000	0.00000	1 Au1	7.49533	66
5.30000	-5.30000	0.00000	1 Au1	7.49533	67
-5.30000	-5.30000	0.00000	1 Au1	7.49533	68
5.30000	0.00000	5.30000	1 Au1	7.49533	69
-5.30000	0.00000	5.30000	1 Au1	7.49533	70
0.00000	5.30000	5.30000	1 Au1	7.49533	71
0.00000	-5.30000	5.30000	1 Au1	7.49533	72
5.30000	0.00000	-5.30000	1 Au1	7.49533	73
-5.30000	0.00000	-5.30000	1 Au1	7.49533	74
0.00000	5.30000	-5.30000	1 Au1	7.49533	75
0.00000	-5.30000	-5.30000	1 Au1	7.49533	76
-6.62500	3.97500	1.32500	2 O1	7.83881	77
3.97500	-6.62500	1.32500	2 O1	7.83881	78
-1.32500	3.97500	6.62500	2 O1	7.83881	79
3.97500	-1.32500	6.62500	2 O1	7.83881	80
-3.97500	6.62500	-1.32500	2 O1	7.83881	81
6.62500	-3.97500	-1.32500	2 O1	7.83881	82
-3.97500	1.32500	-6.62500	2 O1	7.83881	83
1.32500	-3.97500	-6.62500	2 O1	7.83881	84
6.62500	1.32500	3.97500	2 O1	7.83881	85
1.32500	6.62500	3.97500	2 O1	7.83881	86
-6.62500	-1.32500	-3.97500	2 O1	7.83881	87
-1.32500	-6.62500	-3.97500	2 O1	7.83881	88

END

References:

1. J. Szlachetko, M. Nachtegaal, E. de Boni, M. Willimann, O. Safonova, J. Sa, G. Smolentsev, M. Szlachetko, J. A. van Bokhoven, J.-Cl. Dousse, J. Hoszowska, Y. Kayser, P. Jagodzinski, A. Bergamaschi, B. Schmitt, C. David, A. Lücke, Rev. Sci. Instrum. 83, 103105 (2012).
2. A. Bergamaschi, A. Cervellino, R. Dinapoli, F. Gozzo, B. Henrich, I. Johnson, P. Kraft, A. Mozzanica, B. Schmitt, and X. Shi, J. Synchrotron Radiat. 17, 653 (2010).
3. J. L. Campbell, T. Papp, At. Data Nucl. Data Tables 77, 50 (2001).
4. P. Comon, Signal Processing, 36, 287–314 (1994)
5. B. T. Luke, Data Handling in Science and Technology, 23, 3-54 (2003).

6. Yang, W. Y., Cao, W., Chung, T.-S. and Morris, J. Optimization, in Applied Numerical Methods Using MATLAB®, John Wiley & Sons, Inc., Hoboken, NJ, USA. doi: 10.1002/0471705195.ch7 (2005).
7. H. Q. Shi, R. Asahi, C. Stampfl, Phys. Rev. B 75, 205125 (2007)
8. a) G. Kresse, J. Furthmüller, Comput. Mater. Sci. 6, 15 (1996); b) G. Kresse, J. Furthmüller, Phys. Rev. B 54, 11169 (1996); c) G. Kresse, D. Joubert, Phys. Rev. B 59, 1758 (1999); d) P. E. Blöchl, Phys. Rev. B 50, 17953 (1994).
9. J. P. Perdew, J. A. Chevary, S. H. Vosko, K. A. Jackson, M. R. Pederson, D. J. Singh, C. Fiolhais, Phys. Rev. B 46, 6671 (1992).
10. K. Reuter, M. Scheffler, Phys. Rev. B 65, 035406 (2001).